Tunable Rare Earth fcu -MOF Platform: Access to Adsorption Kinetics Driven Gas/Vapor Separations via Pore Size Contraction

ARTICLE *in* JOURNAL OF THE AMERICAN CHEMICAL SOCIETY · MARCH 2015

Impact Factor: 12.11 · DOI: 10.1021/ja5131403 · Source: PubMed

7 AUTHORS, INCLUDING:

Youssef Belmabkhout
King Abdullah University of Science and Techn…
58 PUBLICATIONS **2,443** CITATIONS
SEE PROFILE

Osama Shekhah
King Abdullah University of Science and Techn…
82 PUBLICATIONS **2,549** CITATIONS
SEE PROFILE

Hao Jiang
King Abdullah University of Science and Techn…
2 PUBLICATIONS **5** CITATIONS
SEE PROFILE

Karim Adil
King Abdullah University of Science and Techn…
67 PUBLICATIONS **573** CITATIONS
SEE PROFILE

JACS
JOURNAL OF THE AMERICAN CHEMICAL SOCIETY
Article
pubs.acs.org/JACS

Tunable Rare Earth fcu-MOF Platform: Access to Adsorption Kinetics Driven Gas/Vapor Separations via Pore Size Contraction

Dong-Xu Xue, Youssef Belmabkhout, Osama Shekhah, Hao Jiang, Karim Adil, Amy J. Cairns, and Mohamed Eddaoudi*

Functional Materials Design, Discovery and Development Research Group (FMD^3), Advanced Membranes and Porous Materials Center (AMPM), Division of Physical Sciences and Engineering, King Abdullah University of Science and Technology (KAUST), Thuwal 23955-6900, Kingdom of Saudi Arabia

Supporting Information

ABSTRACT: Reticular chemistry approach was successfully employed to deliberately construct new rare-earth (RE, i.e., Eu^{3+}, Tb^{3+}, and Y^{3+}) **fcu** metal−organic frameworks (MOFs) with restricted window apertures. Controlled and selective access to the resultant contracted **fcu**-MOF pores permits the achievement of the requisite sorbate cutoff, ideal for selective adsorption kinetics based separation and/or molecular sieving of gases and vapors. Predetermined reaction conditions that permitted the formation *in situ* of the 12-connected RE hexanuclear molecular building block (MBB) and the establishment of the first RE-**fcu**-MOF platform, especially in the presence of 2-fluorobenzoic acid (2-FBA) as a modulator and a structure directing agent, were used to synthesize isostructural RE-1,4-NDC-**fcu**-MOFs based on a relatively bulkier 2-connected bridging ligand, namely 1,4-naphthalenedicarboxylate (1,4-NDC). The subsequent RE-1,4-NDC-**fcu**-MOF structural features, contracted windows/pores and high concentration of open metal sites combined with exceptional hydrothermal and chemical stabilities, yielded notable gas/solvent separation properties, driven mostly by adsorption kinetics as exemplified in this work for *n*-butane/methane, butanol/methanol, and butanol/water pair systems.

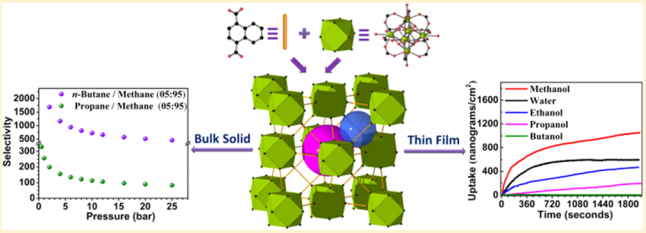

INTRODUCTION

Metal−organic frameworks (MOFs), a special class of solid-state materials, continue to attract remarkable attention in academia and industry alike as prospective functional materials for various key applications due in part to their (i) crystalline nature allowing precise structural determination and subsequent structure−property relationship; (ii) unparalleled permanent porosities, surface areas, and pore volumes, with tunable surface functionalities; and (iii) modularity and amenability to isoreticular chemistry as a result of the practically implemented building block strategies.[1] Markedly, MOF crystal chemistry had permitted access to myriad MOF materials with diverse pore sizes. Nevertheless most of the accomplished pore system tuning was directed toward increasing the pore size rather than contracting it.[2] Certainly, advances in MOF crystal chemistry offer potential to fine-tune the pore apertures to selectively discriminate molecules based on their molecular dimensions, a prerequisite for molecular sieving based gas/vapor/liquid separations. The ability to construct MOFs with reduced pore size and/or restricted pore access offer prospective to (i) enhance the pores local charge densities and subsequently accomplish efficient separation at low pressure applications[3] and (ii) discriminate molecules based on their size and/or functionality leading to adsorption kinetics based separations.[4]

In a recent contribution, we reported the discovery of the 12-connected RE-**fcu**-MOF platform constructed from the assembly of RE hexanuclear molecular building blocks (MBBs) with a series of fluorinated and nonfluorinated, heterofunctional as well as fluorinated homofunctional linkers assisted by the modulator approach, i.e., 2-FBA.[5] This MOF platform encloses two types of cages (i.e., tetrahedral and octahedral) whose faces comprise one type of triangular window (delimited by linkers), constituting the sole entrance/access to the inner **fcu**-MOF pore system for guest molecules. Accordingly, controlling the triangular window size and peripheral functionality can permit to contract the pore size and tune the adsorption properties of the resultant isoreticular **fcu**-MOF and thus unveil MOF sorbents where gas separation can be governed partially (synergy between both adsorption kinetics and adsorption thermodynamics) or totally driven by adsorption kinetics (molecular sieving).

Our previous adsorption studies on the parent RE-**fcu**-MOF revealed the occurrence of a unique synergetic effect involving the polarized 2-fluoro-4-(1*H*-tetrazol-5-yl)benzoic acid (FTZB) ligand (Figures S1−2) containing tetrazolate and fluoro moieties, in proximity of the RE metal centers, to afford enhanced CO_2 adsorption equilibrium selectivity (i.e., 1051)

Received: December 25, 2014
Published: March 31, 2015

DOI: 10.1021/ja5131403
J. Am. Chem. Soc. 2015, 137, 5034−5040

which is particularly suitable for effective low CO_2 concentration removal. However, prompt saturation of these favorable sites at low CO_2 concentrations led to a decrease in CO_2 selectivity vs N_2 (ca. 16) at intermediate and high CO_2 concentrations. In this case and in light of the relatively large pore size, the gas separation of CO_2 from N_2 (also CH_4) using the aforementioned RE-**fcu**-MOF was mainly driven by the difference in adsorption energetics (interactions), while no difference in adsorption kinetics was observed when increasing the size of the probe molecules, as exemplified in case of CO_2, C_2H_6 and C_3H_8 as adsorbate molecules (Figure S3).

In order to contract the opening of the triangular window and potentially promote adsorption kinetics driven selectivity in RE-**fcu**-MOFs, we opted to use a bulkier bridging linker, namely 1,4-naphthalenedicarboxylate (1,4-NDC). Plausibly, contracted pores in the resultant RE-**fcu**-MOFs can also result in enhanced affinity toward more polarizable molecules (i.e., CO_2, C_2H_6, C_3H_8, and n-C_4H_{10}) or promote sieving of relatively bulkier components than CH_4 from natural gas (NG). Noticeably, methane is the main valuable component of NG and is perceptibly regarded as a plausible alternative to conventional fossil fuels such as gasoline and diesel due to its abundance and its relatively cleaner-combustion features. Nevertheless, cost-effective purification/upgrading of NG remains an ongoing challenge since customarily used cryogenic distillation/fractionation separation techniques are energy-intensive.[6] Accordingly, it is timely to explore MOFs potential for such energy intensive separations either as MOF adsorbents or as MOF membranes.

Such a prospective MOF separation agent, in addition to its efficiency to selectively separate CH_4 from CO_2, C_3H_8, and n-C_4H_{10}, should possesses the necessary hydrothermal and chemical stability in order to be deployed under real-world conditions for NG upgrading. Although many MOFs undergo hydrolysis in the presence of moisture,[7] our RE-**fcu**-MOF platform has proven to satisfy this stability criteria. In addition, the election and successful integration of the 1,4-NDC in the RE-**fcu**-MOF is anticipated to enhance the aforementioned stability as it has been shown that integrating additional hydrophobic moieties into the organic backbone of isoreticular MOFs enhances water stability.[8]

Here we report the synthesis and adsorption properties of a series of isostructural **fcu**-MOFs materials (i.e., Eu^{3+}, Tb^{3+} and Y^{3+}) based on the commercially available 1,4-naphthalenedicarboxylic acid as the bridging ligand. The resulting RE-**fcu**-MOFs encompassing a relatively shorter linker with a bulkier functionality expressed remarkable gas/vapor separation efficiencies and excellent chemical and hydrothermal stability.

RESULTS AND DISCUSSION

Solvothermal reactions between $RE(NO_3)_3{\cdot}xH_2O$ (RE = Eu^{3+}, Tb^{3+}, and Y^{3+}) and 1,4-H_2NDC in a *N*,*N*′-dimethylformamide (DMF)/water solution in the presence of 2-FBA yielded transparent homogeneous polyhedral crystals, formulated by single-crystal X-ray diffraction (SCXRD) studies as $[(CH_3)_2NH_2]_2[RE_6(\mu_3\text{-}OH)_8(1,4\text{-}NDC)_6(H_2O)_6]\cdot(solv)_x$ (RE = Eu^{3+}(**1**), Tb^{3+}(**2**), and Y^{3+}(**3**)). The phase purity of the bulk material was independently confirmed by similarities between the calculated and as-synthesized powder X-ray diffraction (PXRD) patterns (Figures S4a−c). It is worth noting that the peak located at 2θ = 14.2 appears clearly in the experimental PXRD pattern but less evidently in the calculated PXRD pattern. This specific peak corresponds to the [222] diffraction plan as it is clearly supported by the Le Bail refinement performed using the FullProf software and hence undoubtedly confirming that the noticed absence of intensity at 2θ = 14.2 is due to accidental extinction (Figure S4d).[9]

Herein **1** is particularly addressed in details since the three compounds are isostructural. Compound **1** crystallizes in the cubic space group $Fm\bar{3}m$. Each Eu^{3+} metal ion is surrounded by four μ_3-OH groups and four oxygen atoms from distinct carboxylate groups from four independent 1,4-NDC^{2-} ligands, leaving the ninth coordination site for a water molecule (Figure 1). The adjacent Eu^{3+} ions are bridged via μ_3-OH and

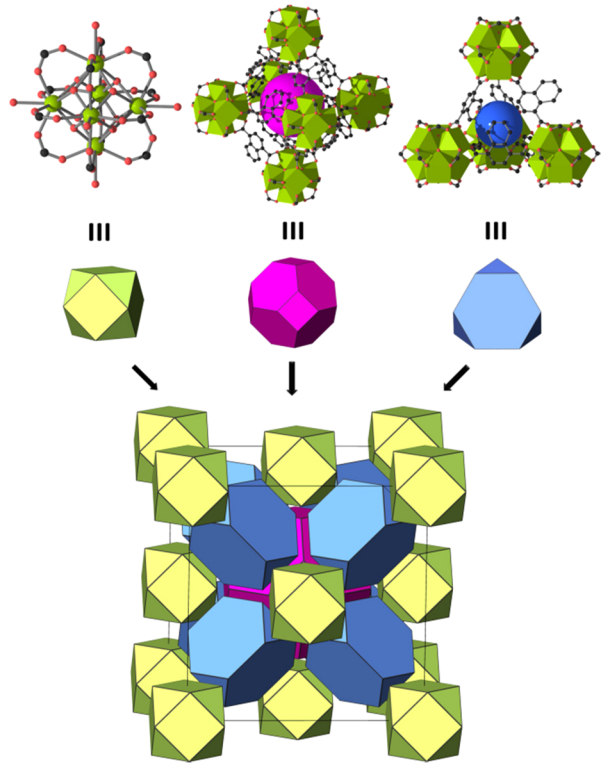

Figure 1. Ball-and-stick and schematic representation of **1**: 12-connected Eu-based MBB and the octahedral and tetrahedral cages with respective pink and blue spheres representing the cavities (top), and the corresponding cuboctahedron node, truncated octahedral and tetrahedral cages (middle) to afford the augmented **fcu** natural tiling (bottom). Eu = lime, C = black, and O = red. Hydrogen atoms and solvent molecules are omitted for clarity.

deprotonated carboxylate groups in a bis-monodentate fashion to give a $[Eu_6(\mu_3\text{-}OH)_8(O_2C-)_{12}]$, a 12-connected MBB. Each hexanuclear MBB is bridged through 1,4-NDC^{2-} anion to produce a 3-periodic MOF (Figure 1). Topological analysis of the resulting crystal structure reveals that **1** is a MOF with the anticipated **fcu** topology constructed from the bridged hexanuclear clusters, $[Eu_6(\mu_3\text{-}OH)_8(O_2C-)_{12}]$ MBBs, where the carbon atoms of the coordinated carboxylates, acting as points of extension, coincide with the cuboctahedron vertex figure of the quasiregular face-centered cubic (**fcu**) net.[10] In **1** the structure encloses two distinct polyhedral cages, i.e., octahedral and tetrahedral, with accessible pore diameters depending on the relative orientation of the naphthalene moieties. As commonly observed in various 1,4-NDC based MOFs with high symmetry,[11] the naphthalene ring in **1** is disordered over four positions, and hence, it is difficult to attribute an exact pore size diameter value to each of the two

DOI: 10.1021/ja5131403
J. Am. Chem. Soc. 2015, 137, 5034−5040

cages. As a result, it is more appropriate to consider a pore size diameter for each cage that takes into account the multiple possible orientations of the naphthalene moieties. Correspondingly, the average diameters for octahedral and tetrahedral cages were estimated to be 8.0 and 4.0 Å based on a geometrically optimized structure (forcite module within Materials Studio software). Most importantly, the access to these two cages is only possible via the triangular windows with an absolute minimal size of 2.4 Å and a maximum size of 5 Å (Figure S8).

The chemical stability of **1** in the presence of water, acidic, and basic conditions was investigated, as these conditions are widely recognized as critical parameters for practical use in many key industrial applications. Markedly, compound **1** maintains its structural integrity in boiling water for at least 24 h. This exceptional stability in boiling water was further authenticated by the preservation of the original apparent surface area, as evidenced by the conserved characteristics of the N_2 adsorption isotherm (Figure S9). Encouraged by this unique attribute, we explored the stability of compound **1** under acidic and basic conditions. Structural analysis and adsorption studies revealed that compound **1** is stable in acidic and basic aqueous solutions at room temperature (i.e., pH 3.5 HCl and pH 10 NaOH). Interestingly, boiling these solutions for 24 h did not alter drastically the structure and the adsorption properties of compound **1** as evidenced by the maintained PXRD pattern and the limited decrease in the surface area (Figures 2a and S9). Regarding the thermal stability of **1**, in situ variable temperature (VT)-PXRD patterns show that **1** is stable up to 400 °C under a vacuum (Figure 2b). These results reveal that compound **1** exhibits remarkable stability in contrast to other MOF materials.[12] The exceptional stability of **1** could be ascribed to the strong Eu−O bond (i.e., 2.375 Å) due to the high charge density (Z/r) of europium, combined with the relatively high hydrophobic character of the shorter 1,4-NDC linker bearing $-C_4H_4-$ group and subsequently shielding the $[Eu_6(\mu_3\text{-}OH)_8]$ cluster moieties in **1** from water exposure/attack.

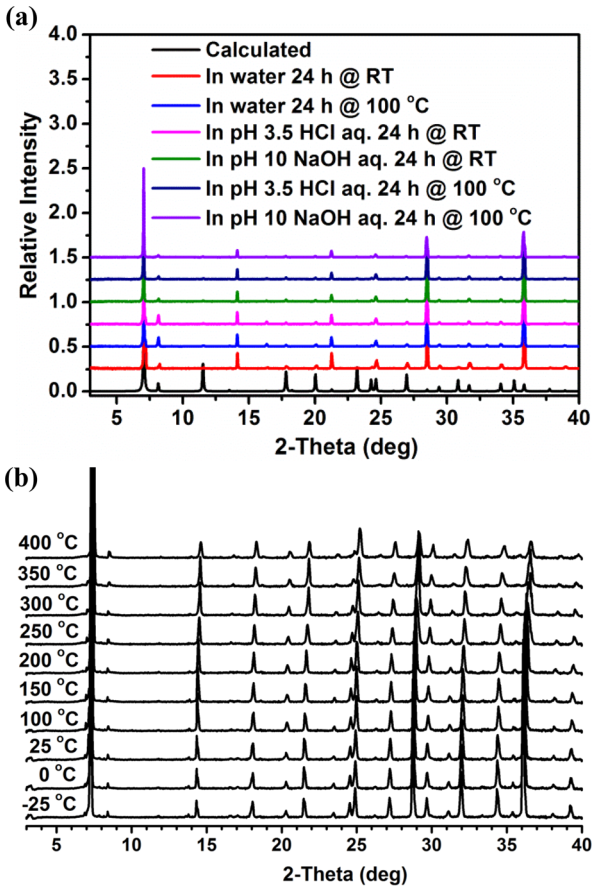

Figure 2. PXRD patterns for **1**: after treatment in water, acidic, and basic conditions for 24 h at room temperature and 100 °C, respectively (a), and in situ VT under a vacuum (b).

The solvent accessible free volume for **1** was estimated to be 39.0%, by summing voxels more than 1.2 Å away from the framework using PLATON software.[13] Argon adsorption studies, initially performed on the methanol-exchanged samples of **1**−**3**, show fully reversible type I isotherms, representative of microporous material with permanent microporosity (Figure S11). The apparent BET surface areas and total pore volumes for **1**−**3** were estimated to be 465 $m^2\ g^{-1}$ and 0.19 $cm^3\ g^{-1}$, 425 $m^2\ g^{-1}$ and 0.18 $cm^3\ g^{-1}$, and 546 $m^2\ g^{-1}$ and 0.22 $cm^3\ g^{-1}$, respectively. To further investigate the adsorption/separation performances of **1**, adsorptions of CO_2, CH_4, N_2, C_2H_6, C_3H_8, and n-C_4H_{10} were carried out. The CO_2 adsorption capabilities were assessed for **1**−**3** at subatmospheric pressures, showing more or less the same uptake at VTs, i.e., 2.01, 1.81, and 2.29 mmol g^{-1} CO_2 at 1 bar and 298 K, respectively (Figure S12). The isosteric heat of adsorption (Q_{st}) as a function of CO_2 loading shows also similar behavior for **1**−**3** (i.e., 34.4, 33.1, and 32.9 kJ mol^{-1} at zero coverage) (Figure S12), which is progressively decreasing as the CO_2 loading increases (i.e., 34.4 to 26.7 kJ mol^{-1} for **1**), indicative of homogeneous binding sites over the full range of gas loading, albeit displaying weaker interactions at low loading as compared to the parent RE **fcu**-MOFs bridged by FTZB linker (i.e., 58.1 kJ mol^{-1}).[5] To further explore the separation capabilities for CO_2 in mixtures with N_2 and CH_4, akin to flue gas and natural gas, respectively, ideal adsorption solution theory (IAST)[14] prediction was carried out on **1** using single gas equilibrium adsorption data of CO_2, N_2, and CH_4 below and above atmospheric pressure (Figure 3a). Interestingly, **1** showed qualitatively much higher CO_2/N_2 (10/90) and CO_2/CH_4 (05/95) selectivity (ca. 82 and 16 at 1 bar, respectively) (Figure 3b) as compared to the parent FTZB-**fcu**-MOF (ca. 16 and 5 at 1 bar, respectively) at relatively higher CO_2 concentration.[5] This can be attributed to the contracted pore size for **1** inducing a considerably higher uniformity of CO_2 adsorption sites while maintaining relatively fast kinetics for CO_2, N_2, and CH_4 similar to the case of FTZB-**fcu**-MOF (Figure S3). In spite of the contracted aperture (<5 Å), the CO_2 selective adsorption vs N_2 and CH_4 is still mainly driven by the preferential interaction of CO_2 with the framework of **1** as compared to N_2 and CH_4. In light of this result, we envisioned to explore further the adsorption and kinetics of a slightly larger and more polarizable probe molecules such as C_2H_6, C_3H_8, n-C_4H_{10}, and iso-C_4H_{10} (Figures 4 and 5). Interestingly, it was found that the adsorption kinetics is reduced from CO_2 to n-C_4H_{10} and iso-C_4H_{10} (Figure 5a), which is a desired feature that can be exploited in improving the separation of C_4 from C_1 via cooperative adsorption kinetics mechanism. This was confirmed by fitting the adsorption kinetics data with the linear driving force model and determining the adsorption kinetics coefficients, i.e., $3.5 \times 10^{-3}\ s^{-1}$ for ethane, $2.1 \times 10^{-3}\ s^{-1}$ for propane, and $8.0 \times 10^{-4}\ s^{-1}$ for n-butane (Table S2).

DOI: 10.1021/ja5131403
J. Am. Chem. Soc. 2015, 137, 5034−5040

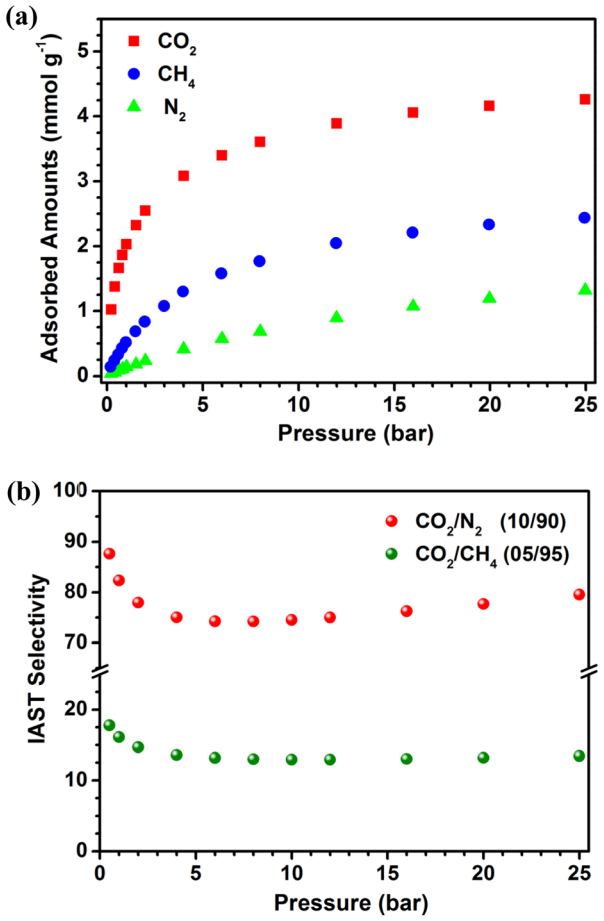

Figure 3. High-pressure adsorption isotherms of **1** for CO_2, CH_4, and N_2 at 298 K (a) and CO_2 adsorption selectivity of **1** for CO_2/N_2 (10:90) and CO_2/CH_4 (05:95) as calculated using IAST at 298 K (b).

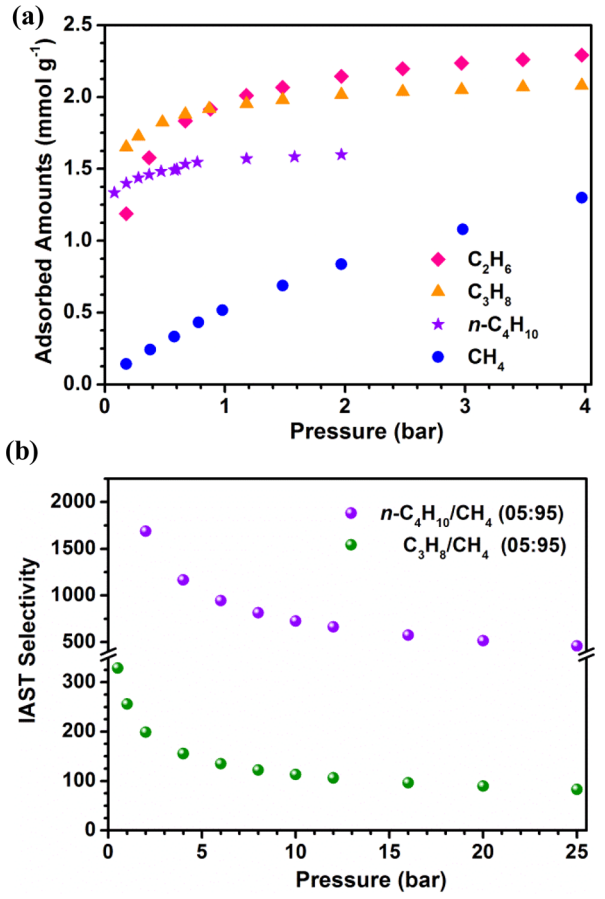

Figure 4. High-pressure adsorption isotherms of **1** for C_2H_6, C_3H_8, and n-C_4H_{10} compared with CH_4 at 298 K (a) and C_{2+} adsorption selectivity of **1** for C_3H_8/CH_4 (05:95) and n-C_4H_{10}/CH_4 (05:95) as calculated using IAST at 298 K (b).

The C_2H_6, C_3H_8, and n-C_4H_{10} equilibrium adsorption measurements were performed up to 4 bar considering their more polarizing attribute and bigger kinetic diameters. Noteworthy, the ethane, propane, and n-butane adsorption isotherms in the low pressure are steeper than the corresponding isotherm of methane (Figure 4a), indicating a relatively stronger affinity between C_{2+} hydrocarbons and the framework of **1**.

Conceivably, in an open MOF material with large pores, the gas adsorbate condensability rises with the increase in the associated gas boiling point (i.e., increasing the number of carbons), and accordingly the strength of the gas-sorbent interactions, at very low partial pressures, increases with the carbon chain length and thus follows the sequence $C_4 > C_3 > C_2 > C_1$. As an illustrative example, the parent Yttrium based FTZB-**fcu**-MOF obeys the gas condensability rationale and thus exhibits a C_3H_8/CH_4 (05/95) equilibrium selectivity of 51 at 1 bar and 298 K (Figure S14a). Upon pore contraction in **1**, the C_3H_8/CH_4 (05/95) equilibrium selectivity increased to ca. 260 under the same conditions. This is driven mainly by the increase of charge density, resulting from the combination of reduced pore size and the relatively bulkier naphthalene moieties. Moreover, this pore contraction effect led to the achievement of very high equilibrium selectivity (ca. 1750 and 2710) for n-C_4H_{10}/CH_4 (05/95) and n-C_4H_{10}/CH_4 (02/98) gas mixtures, respectively, at 2 bar and 298 K calculated using IAST (Figures 4b and S15). This distinctive result was further confirmed experimentally using column breakthrough tests for n-C_4H_{10}/CH_4 (02/98) mixture with almost an infinite selectivity taking into account the setup uncertainties (Figure 5b). In fact, when using a stream of 5 cm^3 min^{-1} of the n-C_4H_{10}/CH_4 (02/98) mixture, the breakthrough time for CH_4 occurred rapidly, while n-C_4H_{10} breakthrough through the column only after 1190 s. Because of the low retention time (in 140 mg of **1**) for CH_4, the quantitative estimation of CH_4 adsorbed is associated with a large percentage of errors, which in turn affect the accuracy of the n-C_4H_{10}/CH_4 selectivity when it is higher than 1000. The plausible interplay between the relatively favorable n-C_4H_{10}–sorbent interactions and the considerably slower adsorption kinetics for n-C_4H_{10} vs CH_4 can potentially explain the observed high n-C_4H_{10}/CH_4 selectivity (2385 ± 300) (the calculated error on the n-C_4H_{10}/CH_4 selectivity is determined without considering the errors associated with the low CH_4 uptake). Encouragingly, the use of 1,4-NDC based RE **fcu**-MOF as a separation agent (with equilibrium or/and kinetics based mechanism) for n-C_4H_{10}/CH_4 offers potential for real industrial applications and should be explored.

In light of the exceptional stability of **1** and its associated distinctive gas adsorption equilibrium and kinetics properties, we further explored its potential for applications pertaining to thin films.[15] Accordingly, we were successful in growing a highly oriented thin film of **1** using in situ crystallization method on a gold surface functionalized with an –OH-

DOI: 10.1021/ja5131403
J. Am. Chem. Soc. 2015, 137, 5034–5040

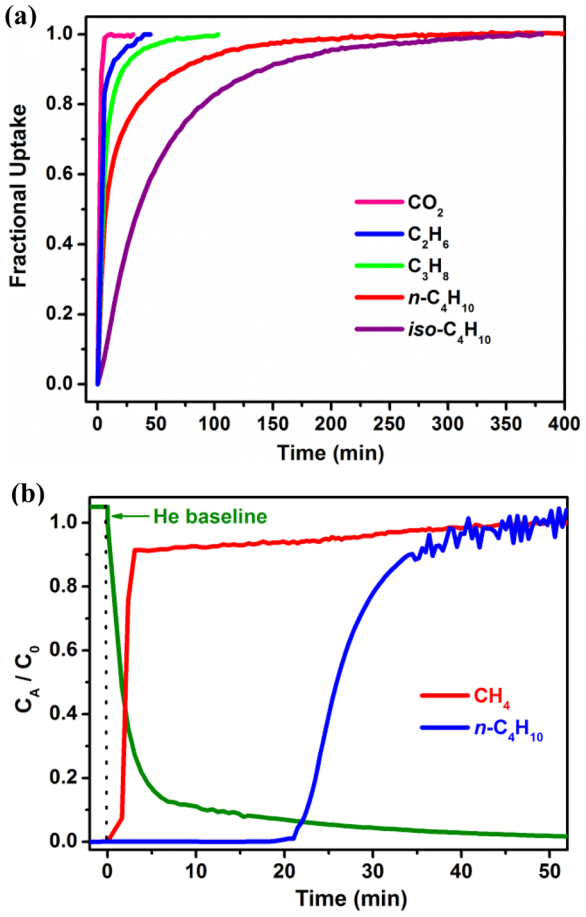

Figure 5. Fractional uptake of CO_2 C_2H_6, C_3H_8, *n*-C_4H_{10}, and *iso*-C_4H_{10} for **1** collected at various pressures (a) and breakthrough test of *n*-C_4H_{10}/CH_4 (02/98) gas mixture at 298 K and 1 bar for **1**(b).

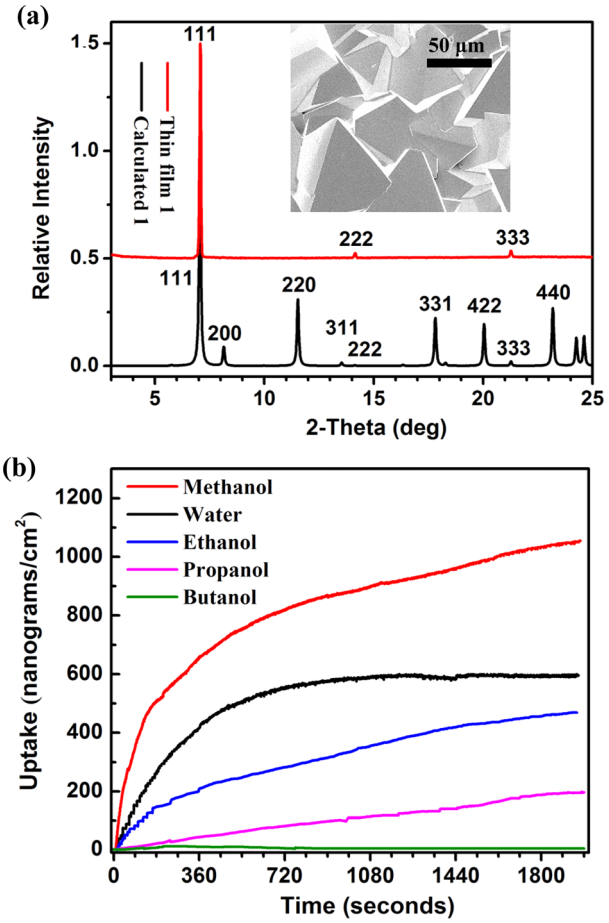

Figure 6. PXRD patterns of **1** calculated and thin-film grown on the −OH-terminated self-assembled monolayer surface (inset is SEM image of thin-film **1** after 24 h of growth) (a) and QCM profiles of specific mass uptake of VOCs at the saturated vapor pressure at room temperature for thin film **1** (b).

terminated surface by using 11-mercaptoundecanol as a self-assembled monolayer (SAM). The thin-film crystallinity and orientation along the [111] direction were confirmed by out-of-plane PXRD pattern (Figure 6a), with reference to the lattices parallel to the surface. This approach to the growth of thin films resulted in the exposure of the triangular windows of the **fcu**-MOF structure (Figure S17a).

The deposition of **1** directly on the quartz crystal microbalance (QCM) gold substrate allowed us to study the adsorption kinetics of volatile organic compounds (VOCs) such as alcohols of different molecular weight at their corresponding vapor pressure at 298 K. The ultrasensitivity of the QCM device permitted to detect mass changes in the nanogram range[15] and allowed further assessment of the adsorption and kinetic selectivity of variable VOCs like methanol, water, ethanol, propanol, and butanol on **1** in the form of a thin film. As evident in Figure 6b, the associated increase in the molecular weight of the alcohols resulted in a clear decrease in the associated adsorption kinetic rate. Indeed, the fastest and highest uptake was found for methanol, while negligible uptake was detected for butanol under similar experimental conditions. Water, the smallest probe molecule studied, was observed to adsorb faster than all alcohols at the steady state (reached at 750 s). This indicates that the resultant thin films of **1** with crystallites orientated in the [111] direction with openings perpendicular to the exposed substrate particularly favored a faster adsorption/uptake of the methanol and water guest molecules. This distinct finding based on adsorption kinetics separation is ideal for removal of butanol from water and/or methanol. Correspondingly, work is in progress to fabricate the **fcu**-MOF associated continuous membrane on a porous support and explore its potential for drying and separation of alcohols as well as for separation of other bulkier molecules.

CONCLUSION

Our quest for partially and/or totally adsorption kinetics driven separations using MOFs led us to employ a bulkier ligand, 1,4-NDC, to assemble new isostructural RE **fcu**-MOFs with restricted pore access. The synthesis of the new isostructural RE **fcu**-MOFs, based on 1,4-NDC, was once again achieved using 2-FBA as a modulator and a structure directing agent for the *in situ* formation of the desired 12-connected MBB, $[RE_6(\mu_3\text{-}OH)_8(O_2C-)_{12}$. Structural features of the resultant RE-**fcu**-MOFs, i.e., relatively shorter linker, 1,4-NDC, bearing hydrophobic $-C_4H_4-$ moiety integrated into the benzene ring, yielded a robust porous material having a high degree of thermal and chemical stability with a structurally smaller/contracted triangular window aperture. Consequently, the resultant RE-**fcu**-MOF, **1**, expressed a relatively higher CO_2/N_2 and CO_2/CH_4 selectivity than the parent **fcu**-MOF constructed using FTZB ligand. Principally, the contracted

DOI: 10.1021/ja5131403
J. Am. Chem. Soc. 2015, 137, 5034−5040

triangular aperture, originated by the bulkiness of the use of 1,4-NDC, resulted in an exceptionally high selectivity of *n*-C_4H_{10} vs CH_4 governed by a complex interplay between thermodynamics and kinetics. Similarly, adsorption kinetic measurements on the associated thin film, grown on gold substrate, showed an unprecedented sieving of butanol from water and other relatively smaller alcohols. The outstanding chemical and thermal stability of the 1,4-NDC based **fcu**-MOFs combined with its associated gas selectivity render this class of **fcu**-MOF material potential candidates for NG upgrading and butanol separation/dehydration. Work is in progress to fabricate the **fcu**-MOF associated continuous membrane on a porous support and explore its potential for gas and/or vapors separations.

EXPERIMENTAL SECTION

Materials and Methods. All reagents were obtained from commercial sources and used without further purification. Fourier-transform infrared (FT-IR) data (4000−600 cm^{-1}) were collected in the solid state on a Nicolet 700 FT-IR spectrometer. The peak intensities are described in each of the spectra as very strong (vs), strong (s), medium (m), weak (w). PXRD measurements were performed on a PANalytical X'Pert PRO MPD X-ray diffractometer at 45 kV, 40 mA for CuKα (λ = 1.5418 Å) equipped with a VT stage, with a scan speed of 2°/min. The sample was held at the designated temperatures for at least 10 min between each scan. High-resolution dynamic thermogravimetric analysis (TGA) was performed under a continuous N_2 flow and recorded on a TA Instruments Hi-Res TGA Q500 Thermogravimetric Analyzer with a heating rate of 5 °C per minute. Low-pressure gas adsorption measurements were performed on a fully automated Autosorb-1C gas adsorption analyzer (Quantachrome Instruments). High-pressure gas adsorption studies were performed on a Magnetic Suspension Balance marketed by Rubotherm (Germany). The SEM images were recorded on a Quanta 600 FEG scanning electron microscope at 30 kV. SCXRD data were collected on Bruker X8 PROSPECTOR APEX2 CCD diffractometers (CuKα, λ = 1.54178 Å).

Synthesis of Compounds. *Synthesis of Eu-1,4-NDC-MOF (**1**).* 1,4-H_2NDC (9.41 mg, 0.0435 mmol), $Eu(NO_3)_3{\cdot}5H_2O$ (18.6 mg, 0.0435 mmol), 2-fluorobenzoic acid (48.7 mg, 0.348 mmol), DMF (2.2 mL), H_2O (0.5 mL), and HNO_3 (0.3 mL, 3.5 M in DMF) were combined in a 20 mL scintillation vial, sealed, and heated to 115 °C for 60 h and cooled to room temperature. The colorless polyhedral crystals were collected and air-dried. FT-IR (4000−600 cm^{-1}): 3300(br), 1653(s), 1600(vs), 1513(s), 1461(s), 1412(vs), 1366(vs), 1264(s), 1211(m), 1165(m), 1098(m), 1031(m), 1020(m), 977(m), 872(m), 848(m), 824(s), 793(vs), 772(m), 745(m), and 662(s).

*Synthesis of Tb-1,4-NDC-MOF (**2**).* 1,4-H_2NDC (9.42 mg, 0.0435 mmol), $Tb(NO_3)_3{\cdot}5H_2O$ (18.9 mg, 0.0435 mmol), 2-fluorobenzoic acid (48.7 mg, 0.348 mmol), DMF (2.2 mL), H_2O (0.5 mL), and HNO_3 (0.3 mL, 3.5 M in DMF) were combined in a 20 mL scintillation vial, sealed, and heated to 115 °C for 60 h and cooled to room temperature. The colorless polyhedral crystals were collected and air-dried. FT-IR (4000−600 cm^{-1}): 3305(br), 1657(s), 1600(vs), 1513(s), 1462(s), 1413(vs), 1364(vs), 1265(s), 1213(m), 1164(m), 1098(m), 1060(m), 1020(w), 977(w), 870(m), 825(m), 793(vs), 772(m), 745(m) and 663(s).

*Synthesis of Y-1,4-NDC-MOF (**3**).* 1,4-H_2NDC (9.40 mg, 0.0435 mmol), $Y(NO_3)_3{\cdot}6H_2O$ (16.7 mg, 0.0435 mmol), 2-fluorobenzoic acid (48.7 mg, 0.348 mmol), DMF (2.2 mL), H_2O (0.5 mL), and HNO_3 (0.3 mL, 3.5 M in DMF) were combined in a 20 mL scintillation vial, sealed, and heated to 115 °C for 60 h and cooled to room temperature. The colorless polyhedral crystals were collected and air-dried. FT-IR (4000−600 cm^{-1}): 3303(br), 1659(s), 1599(vs), 1513(m), 1462(s), 1413(vs), 1369(vs), 1265(s), 1213(m), 1164(m), 1098(m), 1033(m), 1021(w), 978(w), 869(m), 825(s), 793(vs), 772(m), 746(m) and 667(s).

Column Breakthrough Experiments. The stainless steel column used in the breakthrough test is 27 mm in length with 4 mm of inner (6.4 mm outer) diameter. The column downstream is monitored using a Hiden mass spectrometer. In a typical experiment, 0.1−0.4 g of adsorbent was treated at 433 K overnight in vacuum (in oven). After backfill with argon, the column is then transferred to a thermostatic room where helium is flushed trough the column at 5 cm^3 min^{-1}. The gas flow is then switched to the desired *n*-C_4H_{10}/CH_4 (02/98) gas mixture at the same flow rate. The complete breakthrough of C_4H_{10} and CH_4 and other species was indicated by the downstream gas composition reaching that of the feed gas.

Thin-Film Preparation and QCM Measurements. Gold substrate (200 nm Au/2 nm Ti evaporated on Si wafers) was first functionalized with SAMs of 11-mercaptoundecanol (MUD). Then 1,4-H_2NDC (56.38 mg, 0.261 mmol), $Eu(NO_3)_3{\cdot}5H_2O$ (111.72 mg, 0.261 mmol), 2-fluorobenzoic acid (302.4 mg, 2.1 mmol), DMF (3.9 mL), H_2O (0.5 mL), and HNO_3 (0.6 mL, 3.5 M in DMF) were combined in a 50 mL scintillation bottle and completely dissolved, sealed, and heated to 115 °C for 12 h. The mother solution was then cooled to 85 °C. The freshly prepared substrate was then placed vertically in above solution and sealed and heated to 85 °C for another 24 h. The QCM measurements were carried out using a Q-Sense E4 QCM-D instrument and a homemade volatile organic compound vapor dosing system, using N_2 as a carrier gas. The N_2 flux was controlled using a mass flow controller, and the experiments were done using a flow rate of 10 mL/min.

ASSOCIATED CONTENT

Supporting Information

PXRD, TGA, additional structural figures, low- and high-pressure gas adsorption isotherms, IAST, kinetics, and SEM images as well as X-ray crystallographic data. This material is available free of charge via the Internet at http://pubs.acs.org.

AUTHOR INFORMATION

Corresponding Author

*mohamed.eddaoudi@kaust.edu.sa

Notes

The authors declare no competing financial interest.

ACKNOWLEDGMENTS

The authors gratefully acknowledge financial support from King Abdullah University of Science and Technology (KAUST), Kingdom of Saudi Arabia.

REFERENCES

(1) (a) Eddaoudi, M.; Moler, D. B.; Li, H.; Chen, B.; Reineke, T. M.; O'Keeffe, M.; Yaghi, O. M. *Acc. Chem. Res.* **2001**, *34*, 319. (b) Ferey, G. *J. Solid State Chem.* **2000**, *152*, 37. (c) Kitagawa, S.; Kitaura, R.; Noro, S. *Angew. Chem., Int. Ed.* **2004**, *43*, 2334. (d) Eddaoudi, M.; Kim, J.; Rosi, N.; Vodak, D.; Wachter, J.; O'Keeffe, M.; Yaghi, O. M. *Science* **2002**, *295*, 469. (e) Eubank, J. F.; Nouar, F.; Luebke, R.; Cairns, A. J.; Wojtas, L.; Alkordi, M.; Bousquet, T.; Hight, M. R.; Eckert, J.; Embs, J. P.; Georgiev, P. A.; Eddaoudi, M. *Angew. Chem., Int. Ed.* **2012**, *51*, 10099. (f) Zhang, Y. B.; Zhou, H. L.; Lin, R. B.; Zhang, C.; Lin, J. B.; Zhang, J. P.; Chen, X. M. *Nat. Commun.* **2012**, *3*, 642. (g) Cook, T. R.; Zheng, Y. R.; Stang, P. J. *Chem. Rev.* **2013**, *113*, 734. (h) Chun, H.; Dybtsev, D. N.; Kim, H.; Kim, K. *Chem.—Eur. J.* **2005**, *11*, 3521. (i) Zhao, D.; Timmons, D. J.; Yuan, D. Q.; Zhou, H. C. *Acc. Chem. Res.* **2011**, *44*, 123. (j) Sun, Q. F.; Sato, S.; Fujita, M. *Nature Chem.* **2012**, *4*, 330. (k) Ma, L. Q.; Falkowski, J. M.; Abney, C.; Lin, W. B. *Nature Chem.* **2010**, *2*, 838. (l) Dinca, M.; Dailly, A.; Liu, Y.; Brown, C. M.; Neumann, D. A.; Long, J. R. *J. Am. Chem. Soc.* **2006**, *128*, 16876. (m) Masciocchi, N.; Galli, S.; Colombo, V.; Maspero, A.; Palmisano, G.; Seyyedi, B.; Lamberti, C.; Bordiga, S. *J. Am. Chem. Soc.* **2010**, *132*, 7902. (n) Padial, N. M.; Procopio, E. Q.; Montoro, C.; Lopez, E.; Oltra, J. E.; Colombo, V.; Maspero, A.; Masciocchi, N.;

DOI: 10.1021/ja5131403
J. Am. Chem. Soc. 2015, 137, 5034−5040

Galli, S.; Senkovska, I.; Kaskel, S.; Barea, E.; Navarro, J. A. R. *Angew. Chem., Int. Ed.* **2013**, *52*, 8290. (o) Schaate, A.; Roy, P.; Preusse, T.; Lohmeier, S. J.; Godt, A.; Behrens, P. *Chem. -Eur. J.* **2011**, *17*, 9320. (p) Furukawa, H.; Cordova, K. E.; O'Keeffe, M.; Yaghi, O. M. *Science* **2013**, *341*, 974. (q) Zhang, J. P.; Zhang, Y. B.; Lin, J. B.; Chen, X. M. *Chem. Rev.* **2012**, *112*, 1001. (r) Guillerm, V.; Weselinski, L. J.; Belmabkhout, Y.; Cairns, A. J.; D'Elia, V.; Wojtas, L.; Adil, K.; Eddaoudi, M. *Nature Chem.* **2014**, *6*, 673. (s) Guillerm, V.; Kim, D.; Eubank, J. F.; Luebke, R.; Liu, X.; Adil, K.; Lah, M. S.; Eddaoudi, M. *Chem. Soc. Rev.* **2014**, *43*, 6141.

(2) Furukawa, H.; Ko, N.; Go, Y. B.; Aratani, N.; Choi, S. B.; Choi, E.; Yazaydin, A. O.; Snurr, R. Q.; O'Keeffe, M.; Kim, J.; Yaghi, O. M. *Science* **2010**, *329*, 424. Deng, H. X.; Grunder, S.; Cordova, K. E.; Valente, C.; Furukawa, H.; Hmadeh, M.; Gandara, F.; Whalley, A. C.; Liu, Z.; Asahina, S.; Kazumori, H.; O'Keeffe, M.; Terasaki, O.; Stoddart, J. F.; Yaghi, O. M. *Science* **2012**, *336*, 1018. Farha, O. K.; Eryazici, I.; Jeong, N. C.; Hauser, B. G.; Wilmer, C. E.; Sarjeant, A. A.; Snurr, R. Q.; Nguyen, S. T.; Yazaydin, A. O.; Hupp, J. T. *J. Am. Chem. Soc.* **2012**, *134*, 15016. Yun, R.; Lu, Z.; Pan, Y.; You, X.; Bai, J. *Angew. Chem., Int. Ed.* **2013**, *52*, 11282. An, J.; Farha, O. K.; Hupp, J. T.; Pohl, E.; Yeh, J. I.; Rosi, N. L. *Nat. Commun.* **2012**, *3*, 604. Song, X.; Kim, T. K.; Kim, H.; Kim, D.; Jeong, S.; Moon, H. R.; Lah, M. S. *Chem. Mater.* **2012**, *24*, 3065.

(3) Nugent, P.; Belmabkhout, Y.; Burd, S. D.; Cairns, A. J.; Luebke, R.; Forrest, K.; Pham, T.; Ma, S. Q.; Space, B.; Wojtas, L.; Eddaoudi, M.; Zaworotko, M. J. *Nature* **2013**, *495*, 80.

(4) Li, K. H.; Olson, D. H.; Seidel, J.; Emge, T. J.; Gong, H. W.; Zeng, H. P.; Li, J. *J. Am. Chem. Soc.* **2009**, *131*, 10368.

(5) Xue, D.-X.; Cairns, A. J.; Belmabkhout, Y.; Wojtas, L.; Liu, Y.; Alkordi, M. H.; Eddaoudi, M. *J. Am. Chem. Soc.* **2013**, *135*, 7660.

(6) Cavenati, S.; Grande, C. A.; Rodrigues, A. E. *Energy Fuels* **2006**, *20*, 2648. He, Y. B.; Zhou, W.; Krishna, R.; Chen, B. L. *Chem. Commun.* **2012**, *48*, 11813.

(7) Kaye, S. S.; Dailly, A.; Yaghi, O. M.; Long, J. R. *J. Am. Chem. Soc.* **2007**, *129*, 14176. Low, J. J.; Benin, A. I.; Jakubczak, P.; Abrahamian, J. F.; Faheem, S. A.; Willis, R. R. *J. Am. Chem. Soc.* **2009**, *131*, 15834.

(8) Nguyen, J. G.; Cohen, S. M. *J. Am. Chem. Soc.* **2010**, *132*, 4560. Wu, T. J.; Shen, L. J.; Luebbers, M.; Hu, C. H.; Chen, Q. M.; Ni, Z.; Masel, R. I. *Chem. Commun.* **2010**, *46*, 6120. Taylor, J. M.; Vaidhyanathan, R.; Iremonger, S. S.; Shimizu, G. K. H. *J. Am. Chem. Soc.* **2012**, *134*, 14338.

(9) Le Bail, A.; Duroy, H.; Fourquet, J. L. *Mater. Res. Bull.* **1988**, *23*, 447. Rodriguez-Carvajal, J. *FullProf: A Program for Rietveld Refinement and Pattern Matching Analysis*; Laboratoire Léon Brillouin, CEA: Gif sur Yvette Cedex France, 1990.

(10) Friedrichs, O. D.; O'Keeffe, M.; Yaghi, O. M. *Acta Crystallogr., Sect. A* **2003**, *59*, 22.

(11) Horike, S.; Matsuda, R.; Tanaka, D.; Matsubara, S.; Mizuno, M.; Endo, K.; Kitagawa, S. *Angew. Chem., Int. Ed.* **2006**, *45*, 7226.

(12) Cavka, J. H.; Jakobsen, S.; Olsbye, U.; Guillou, N.; Lamberti, C.; Bordiga, S.; Lillerud, K. P. *J. Am. Chem. Soc.* **2008**, *130*, 13850. Colombo, V.; Galli, S.; Choi, H. J.; Han, G. D.; Maspero, A.; Palmisano, G.; Masciocchi, N.; Long, J. R. *Chem. Sci.* **2011**, *2*, 1311. Montoro, C.; Linares, F.; Procopio, E. Q.; Senkovska, I.; Kaskel, S.; Galli, S.; Masciocchi, N.; Barea, E.; Navarro, J. A. R. *J. Am. Chem. Soc.* **2011**, *133*, 11888. Guillerm, V.; Ragon, F.; Dan-Hardi, M.; Devic, T.; Vishnuvarthan, M.; Campo, B.; Vimont, A.; Clet, G.; Yang, Q.; Maurin, G.; Ferey, G.; Vittadini, A.; Gross, S.; Serre, C. *Angew. Chem., Int. Ed.* **2012**, *51*, 9267. Liao, P. Q.; Zhou, D. D.; Zhu, A. X.; Jiang, L.; Lin, R. B.; Zhang, J. P.; Chen, X. M. *J. Am. Chem. Soc.* **2012**, *134*, 17380. Jiang, H.-L.; Feng, D.; Wang, K.; Gu, Z.-Y.; Wei, Z.; Chen, Y.-P.; Zhou, H.-C. *J. Am. Chem. Soc.* **2013**, *135*, 13934. Duan, J.; Higuchi, M.; Horike, S.; Foo, M. L.; Rao, K. P.; Inubushi, Y.; Fukushima, T.; Kitagawa, S. *Adv. Funct. Mater.* **2013**, *23*, 3525. Park, K. S.; Ni, Z.; Cote, A. P.; Choi, J. Y.; Huang, R. D.; Uribe-Romo, F. J.; Chae, H. K.; O'Keeffe, M.; Yaghi, O. M. *Proc. Natl. Acad. Sci. U. S. A.* **2006**, *103*, 10186.

(13) Spek, A. L. *Acta Crystallogr.* **1990**, *46*, c34.

(14) Myers, A. L.; Prausnitz, J. M. *AIChE J.* **1965**, *11*, 121.

(15) Shekhah, O.; Liu, J.; Fischer, R. A.; Woll, C. *Chem. Soc. Rev.* **2011**, *40*, 1081. Gu, Z. Y.; Yang, C. X.; Chang, N.; Yan, X. P. *Acc. Chem. Res.* **2012**, *45*, 734.

DOI: 10.1021/ja5131403
J. Am. Chem. Soc. 2015, 137, 5034−5040